Homogeneous nucleation of *n*-nonane and *n*-propanol mixtures: A comparison of classical nucleation theory and experiments

A. I. Gaman[a] and I. Napari
Department of Physical Sciences, University of Helsinki, 00014 Helsinki, Finland

P. M. Winkler
Institut für Experimentalphysik, Universität Wien, Boltzmanngasse 5, A-1090 Wien, Austria

H. Vehkamäki
Department of Physical Sciences, University of Helsinki, 00014 Helsinki, Finland

P. E. Wagner
Institut für Experimentalphysik, Universität Wien, Boltzmanngasse 5, A-1090 Wien, Austria

R. Strey
Institut für Physikalische Chemie, Universität zu Köln, Luxemburger Strasse 116, D-50939 Köln, Germany

Y. Viisanen
Finnish Meteorological Institute, Air Quality Research, Sahaajankatu 20E, 00880 Helsinki, Finland

M. Kulmala
Department of Physical Sciences, University of Helsinki, 00014 Helsinki, Finland

(Received 1 February 2005; accepted 21 October 2005; published online 23 December 2005)

The homogeneous nucleation rates for *n*-nonane–*n*-propanol vapor mixtures have been calculated as a function of vapor-phase activities at 230 K using the classical nucleation theory (CNT) with both rigorous and approximate kinetic prefactors and compared to previously reported experimental data. The predicted nucleation rates resemble qualitatively the experimental results for low *n*-nonane gas phase activity. On the high nonane activity side the theoretical nucleation rates are about three orders of magnitude lower than the experimental data when using the CNT with the approximate kinetics. The accurate kinetics improves the situation by reducing the difference between theory and experiments to two orders of magnitude. Besides the nucleation rate comparison and the experimental and predicted onset activities, the critical cluster composition is presented. The total number of molecules is approximated by CNT with reasonable accuracy. Overall, the classical nucleation theory with rigorous kinetic prefactor seems to perform better. The thermodynamic parameters needed to calculate the nucleation rates are revised extensively. Up-to-date estimates of liquid phase activities using universal functional activity coefficient Dortmund method are presented together with the experimental values of surface tensions obtained in the present study.
 [DOI: 10.1063/1.2138703]

I. INTRODUCTION

The homogeneous nucleation of a vapor is the process through which, in the absence of any kind of surfaces, the first droplets of the liquid phase appear. The nucleation rate depends strongly on temperature and supersaturation, i.e., the ratio of the partial pressure of the nucleating vapor to its equilibrium vapor pressure. The first theory on homogeneous nucleation, known as classical nucleation theory (CNT), was derived by Volmer and Weber[1] and refined to its current form by Frenkel[2] and Zeldovich.[3] A decade and a half later, the binary CNT was derived by Neumann and Döring,[4] who applied it on water-ethanol system (see also Stauffer[5] and Trinkaus[6] for a more accurate description of nucleation kinetics). The unfortunate choice of a system with compositional gradients of surface tension led them to unphysical predictions, i.e., at certain gas phase activities the theory predicts a negative number of water molecules in the critical cluster. Nevertheless, the classical nucleation theory remains a very attractive tool due to its relative simplicity and in spite of the assumption that the cluster comprising of few molecules is characterized by the bulk liquid properties (e.g., density, surface tension, and activities).

Several experimental studies on homogeneous nucleation in different systems, either unary, binary or ternary, have been performed in the last decade,[7–10] providing detailed information about the microscopic aspects of the nucleation process. This information allows us to test the nucleation theories with higher precision. For example, the experiments show that CNT, accepted for many years as essentially correct, agrees fairly well for unary systems of nonpolar molecules[9] but gets worse for binary systems,[11] producing even thermodynamic inconsistencies for nonideal mixtures. This fact leads to the necessity of investigating

[a]Electronic mail: anca.gaman@helsinki.fi

different classes of substances, both experimentally[12,13] and theoretically,[14–19] first in order to develop an adequate quantitative theory and second to determine the ability of different vapors to nucleate and the conditions where they can participate in nucleation processes.

This article is devoted to the comparison of CNT and experimental data of an *n*-nonane–*n*-propanol system. The full set of nucleation rate data is provided by Viisanen *et al.*[9] In their article, the authors present the first measurements of nucleation rates in supersaturated *n*-nonane–*n*-alcohol vapor mixtures using nucleation pulse method. For a detailed description of the experimental procedure we direct the reader to the article of Viisanen *et al.*[9] and the references within.

Separately, *n*-nonane and *n*-propanol have been the subject of several investigations. Hung *et al.*[12] and Adams *et al.*[20] measured the homogeneous nucleation of *n*-nonane as a function of supersaturation for different temperatures. The observed dependences were then compared with predictions of different nucleation theories. Hung *et al.*[12] reported that the closest agreement was obtained with the classical theory of nucleation, although for a perfect agreement a temperature-dependent correction factor was required. Adams *et al.*[20] compared their experimental results with CNT and with CNT with the Reiss, Katz, and Cohen (RKC) replacement factor formulated by Reiss *et al.*[21] and Reiss and Katz.[22] Classical nucleation theory did not predict accurately the nucleation rates of *n*-nonane, while the inclusion of the RKC replacement factor improved the result considerably, although it produced an unphysical sticking coefficient.

Wagner and Strey[10] reported an experimental study of the homogeneous nucleation of an *n*-nonane–water system that exhibits a pronounced miscibility gap in liquid state. In an onset activity plot, the experimental points and the classical nucleation theory exhibited linear portions separated by limited regions of strong curvature. The authors concluded that the nucleation in this system can be viewed as a superposition of two simultaneous unary nucleation processes.

Water–*n*-propanol nucleation rate measurements were reported by Strey *et al.*,[7] as a part of an extended set of data on homogeneous nucleation in water–*n*-alcohol vapor mixtures. The authors emphasized the need of a theory describing homogeneous nucleation for a system with strong nonideal behavior or miscibility gaps.

Several experiments on the heterogeneous nucleation of the water–*n*-propanol system and the comparison with different heterogeneous nucleation theories have also been reported.[23,24] There, the major difficulty consists in determining the contact angle between the parent aerosol particle and the formed embryo and its dependence on the composition of the embryo.

To the authors' knowledge, no theoretical work on the *n*-nonane–*n*-propanol binary nucleation has been reported until now. Viisanen *et al.*[9] did not make any comparison with nucleation theory due to the lack of thermophysical data at that time. They determined the number of molecules in the critical cluster by using solely the slopes of the nucleation rate surface, without reference to any specific nucleation theory.

The following section is devoted to a brief review of classical nucleation theory. The thermophysical properties and the methods of calculating/evaluating the properties of the mixture are presented in Sec. III. In Sec. IV our numerical calculations and the comparison with the experimental data are presented and discussed. Finally, in Sec. V we present our conclusions and prospects for future investigations.

II. THEORY

A. Composition of the critical cluster

Considering a liquidlike cluster containing n_1 molecules of *n*-nonane and n_2 molecules of *n*-propanol (from now on, subscript 1 refers to *n*-nonane and subscript 2 refers to *n*-propanol), the formation energy of the cluster is given by, e.g., Laaksonen *et al.*,[25]

$$\Delta G = -kT\left[n_1 \ln\left(\frac{P_1}{P_{\mathrm{sat},1}}\right) + n_2 \ln\left(\frac{P_2}{P_{\mathrm{sat},2}}\right)\right] + 4\pi\sigma r^2, \quad (1)$$

where P_i is the ambient partial pressure of the free molecules of species i $(i=1,2)$, $P_{\mathrm{sat},i}$ is the equilibrium vapor pressure of species i above a flat solution surface, r is the radius of the droplet, and σ is the surface tension of a flat liquid-vapor interface at the core composition of the nucleus. The particle numbers can be written as $n_i = n_{i,l} + n_{i,s}$, where $n_{i,l}$ is the number of particles in the cluster core and $n_{i,s}$ is the surface excess. The core composition of the critical cluster $x^* = n_{2,l}/(n_{1,l}+n_{2,l})$ is found by requiring $(\partial \Delta G/\partial n_i)_{n_j} = 0$ (the superscript * refers to critical cluster). The resulting equation,

$$\ln\left(\frac{P_1}{P_{\mathrm{sat},1}(x,T)}\right)\upsilon_2(x,T) = \ln\left(\frac{P_2}{P_{\mathrm{sat},2}(x,T)}\right)\upsilon_1(x,T), \quad (2)$$

where υ_i is the partial molar volume of species i, is then solved numerically for x^*. The radius of the critical cluster is obtained then from the Kelvin equation,

$$r^* = \frac{2\sigma\upsilon_i}{kT\ln(P_i/P_{\mathrm{sat},i})}, \quad (3)$$

and the formation energy from

$$\Delta G^* = \frac{4}{3}\pi r^{*2}\sigma. \quad (4)$$

The number of molecules n_1^* and n_2^* in the critical cluster are calculated from

$$n_2^* = \frac{x^*\rho(x^*)\frac{4}{3}\pi r^{*3}}{x^* m_2 + (1-x^*)m_1} \quad (5)$$

and

$$n_1^* = \frac{n_2^*(1-x^*)}{x^*}. \quad (6)$$

The expressions for the excess surface numbers are[26]

$$n_{1s} = \frac{4\pi r^2 2(d\sigma/dx)}{(\upsilon_2/\upsilon_1)(d\mu_{1l}/dx) - (d\mu_{2l}/dx)}, \quad (7)$$

$$n_{2s} = \frac{4\pi r^2 (d\sigma/dx)}{(v_1/v_2)(d\mu_{2l}/dx) - (d\mu_{1l}/dx)}. \tag{8}$$

Here v_i denotes the partial molecular volume of species i, μ_{il} is the chemical potential, and σ is the surface tension.

B. Accurate kinetics

The general form of the nucleation rate is given by[6]

$$I = \frac{|\lambda|/\pi}{\sqrt{-\det(\mathbf{D})/\pi}} \rho(\{n_1^*, n_2^*\}), \tag{9}$$

where $\rho(\{n_i\})$ is the equilibrium distribution of clusters containing n_i molecules of each species, **D** is a matrix with elements

$$D_{ij} = \left. \frac{1}{2kT} \frac{\partial^2 \Delta G(\{n_1, n_2\})}{\partial n_i \partial n_j} \right|_{\{n_i^*\}}, \quad (i,j = 1,2), \tag{10}$$

and λ is the negative eigenvalue of matrix **KD**, where **K** is the condensation matrix,[27]

$$K_{mn} = \sum_{\{n_i'\}}^{\xi} n_m' n_n' k(\{n_i'\}; \{n_i^*\}) \rho(\{n_i'\}), \tag{11}$$

where $k(\{n_i'\}; \{n_i^*\})$ is the rate of collisions between critical clusters of size $(\{n_i^*\})$ and clusters of size $(\{n_i'\})$ and n_m' and n_n' are the numbers of molecules of species m and n $(m,n = 1,2)$ in a cluster of size $(\{n_i'\})$, respectively. The summation in Eq. (11) goes over all clusters up to ξ, which is an upper bound above which cluster-cluster collisions are neglected. In this paper, the colliding clusters are assumed to be n-nonane and n-propanol molecules.

The collision probability is obtained from the kinetic gas theory as

$$k(\{n_i'\}; \{n_i^*\}) = \sqrt{8\pi kT \left(\frac{1}{m^*} + \frac{1}{m'} \right)} (r^* + r')^2, \tag{12}$$

where r^* and r' are the radii of the critical cluster and the colliding cluster (here molecules of n-nonane and n-propanol), respectively, and m^* and m' are the corresponding masses. The equilibrium distribution is given by[28]

$$\rho(\{n_1, n_2\}) = (\rho_1 + \rho_2) \exp\left(\frac{-\Delta G(n_1, n_2)}{kT} \right), \tag{13}$$

where ρ_1 and ρ_2 are the number densities of free n-nonane and n-propnanol molecules.

The CNT and the accurate kinetics will be refered to as CNT(Z1).

C. Approximate kinetics

Usually the kinetics of nucleation is thought to be of minor importance. Here the binary system is reduced to unary system so that the evaluation of the kinetic part of the nucleation rate is easier. The nucleation rate is given by Stauffer,[5]

$$I = R_{\mathrm{AV}}^* Z \rho^*(n_1, n_2), \tag{14}$$

where R_{AV}^* represents the average growth rate. For nonassociating vapors,

$$R_{\mathrm{AV}} = \frac{R_1 R_2}{R_1 \sin^2 \Phi + R_2 \cos^2 \Phi}. \tag{15}$$

The growth rates of individual species R_i are obtained from kinetic gas theory as

$$R_i = \sqrt{\frac{kT}{2\pi m_i}} \rho_{i,v} A^*, \tag{16}$$

where m_i is the mass of molecule i, $\rho_{i,v}$ is the vapor concentration of i, and A^* is the area of the cluster. Φ is the angle between the n_1 axis and the direction of the growth at the saddle point of the free-energy surface. In practice, we approximate Φ by the angle of steepest descent $\Phi \approx n_1^*/n_2^*$. The Zeldovich factor Z is obtained from the second derivatives of ΔG at the saddle point. Here, we apply the concept of virtual monomer,[29] which reduces Z to an approximate expression,

$$Z = \sqrt{\frac{\sigma}{kT}} \frac{v}{2\pi r^{*2}}, \tag{17}$$

where $v = v_1 n_1 + v_2 n_2$ is the volume of the average monomer.

The calculations using CNT and the approximate kinetics will be henceforth refered to as CNT(Z2).

III. THERMOPHYSICAL PROPERTIES

A considerable amount of information on the equilibrium properties of liquid mixtures as a function of temperature and composition is needed before nucleation rates can be calculated. Partial pressures of molecular components above the flat solution surface and the density of the solution are required to obtain the core composition of the critical nucleus from Eq. (2). Furthermore, the surface tension of the mixture is needed to calculate the size of the nucleus from Eq. (3). In the following, we present a detailed account on how these properties were obtained for the n-nonane–n-propanol system.

A. Densities

Several references for densities of pure components can be found in literature. They are in almost perfect agreement (the very small deviations will not affect the theoretical nucleation rates), therefore we provide here only the ones listed by Chemical Properties Handbook,[30] with the density given by

$$\rho_i = AB^{(-(1 - T/T_c)^C)} \ [\mathrm{g/cm^3}], \tag{18}$$

where the constants A, B, and C, the critical temperatures T_c, and the temperature ranges for n-nonane and n-propanol are given in Table I. The density of the mixture can be estimated using the ideal mixture theory as

TABLE I. The constants, critical temperature, and temperature range for pure component density calculation according to Eq. (18) and for pure component vapor pressure according to Eq. (20).

Property	Species	A	B	C	D	E	T_c (K)	$T_{\min}$ (K)	$T_{\max}$ (K)
Density	*n*-nonane	0.233 64	0.255 56	0.285 71	⋯	⋯	595.65	219.63	596.65
	n-propanol	0.276	0.272	0.25	⋯	⋯	536.71	146.95	536.71
Vapor pressure	*n*-nonane	8.8817	−2.8042*E*+03	1.5262*E*+00	−1.0464*E*−02	5.7972*E*−06	⋯	219.63	595.65
	n-propanol	31.5155	−3.4570*E*+03	−7.5235*E*+00	−4.2870*E*−11	1.3029*E*−07	⋯	146.95	536.71

$$\rho_{\text{mixture}} = \frac{M_1 + x(M_2 - M_1)}{\upsilon_1 - x(\upsilon_2 - \upsilon_1)}, \tag{19}$$

where M_1 and M_2 are the molecular masses of the components, x is the *n*-propanol mole fraction, and υ_1 and υ_2 are the molecular volumes assumed to be composition independent and equal to those of the pure components.

B. Vapor pressures

The Antoine-type equation with extended terms was selected for the correlation of pure liquid-vapor pressure with temperature,[30]

$$\log_{10}(\rho) = A + \frac{B}{T} + C\log_{10}(T) + DT + ET^2 \ [\text{mm Hg}], \tag{20}$$

with p=vapor pressure, $A-E$=regression coefficients, and T=temperature [K].[30] The coefficients are given in Table I.

We performed sensitivity tests by changing the formula for vapor pressure. Hung *et al.*[12] present an extended discussion on the effects of *n*-nonane vapor pressure discrepancies, concluding that the expression given by King and Najjar[31] is the most accurate for the temperature range they used. The equilibrium vapor pressure measurements for *n*-propanol from Schmeling and Strey[32] were also considered. Although in their experiments the temperature range has the lower limit at 243 K, we believe that extrapolating down to 230 K—the experimental temperature of Viisanen *et al.*[9]—will not result in very substantial errors. There are small discrepancies in the vapor pressures given by the proposed equations at very low temperatures. However, the differences in the vapor pressures are small enough for the nucleation rate to remain within the same order of magnitude.

C. Surface tension

Unlike the properties listed above, the surface tension of pure components shows relatively large variability in literature data. Evidently, the computed surface tensions for mixture will also display differences which will reflect on the theoretical nucleation rates. As an example, we consider here the surface tensions for pure components from Dean[33] and Wagner and Strey[34] for *n*-nonane and Dean[33] and Strey and Schmeling[35] for *n*-propanol, listed in Table II. A plot of the surface tensions from the above-mentioned references (Fig. 1) as a function of temperature shows a 3.3% difference for nonane at 230 K and of about 1% for propanol at the same temperature. As temperature increases, the differences decrease until about 270 K for *n*-nonane and close to 280 K for propanol when the lines cross each other.

In the present study the surface tensions for *n*-nonane, *n*-propanol, and mixtures with various compositions were measured over a range of temperatures at the Institute for Experimental Physics, University of Vienna.

The experimental data on surface tension have been obtained by applying the Wilhelmy plate method.[36,37] This method is based on the measurement of the force on a roughened platinum plate in contact with the liquid under study. Before each single measurement the plate is immersed into the liquid and subsequently withdrawn until the bottom edge of the plate is at the level of the liquid surface. Thereby, buoyancy effects are eliminated, and the knowledge of the liquid density is not required. If the contact angle of the liquid surface on the plate is zero the surface tension can directly be obtained from the experimentally determined force and the physical dimensions of the plate. In the present study a commercial-process-controlled tensiometer (Krüss, model K12) was used.

Surface tensions for pure *n*-nonane and *n*-propanol were measured in the temperature range of 273–303 K. In this temperature range the absolute experimental error is below

TABLE II. Surface tension of pure *n*-nonane and *n*-propanol.

Pure componenet surface tension	$T_{\min}$ (°C)	$T_{\min}$ (°C)	References
σ_p[N/m]=0.04821−T[K]×0.08394*e*−3	−40	40	Strey and Schmeling[a]
σ_n[erg/cm^2]=24.80−T[°C]×0.1201	extrapolated down to −73.15 °C		Wagner and Strey[b]
σ_p[mN/m]=25.26−0.0777×T[°C]	−127	97.2	Dean[c]
σ_n[mN/m]=27.72−0.0935×T[°C]	−53.5	150.8	Dean[c]

[a]Reference 29.
[b]Reference 28.
[c]Reference 27.

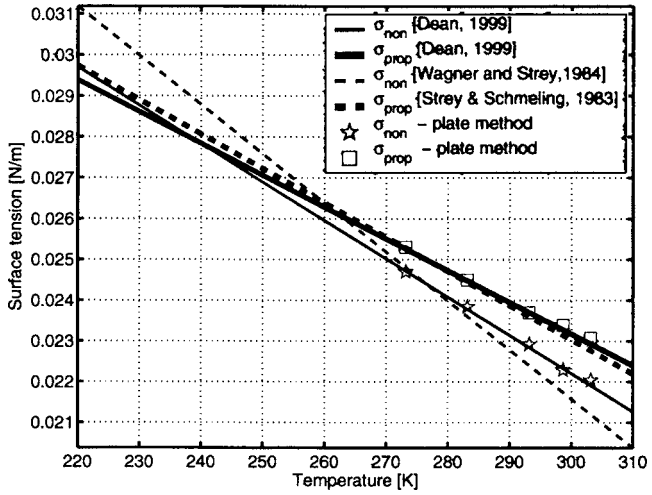

FIG. 1. The surface tension of pure components as a function of temperature according to Wagner and Strey (Ref. 34) and Dean (Ref. 33). The experimental data obtained using plate method (see the text for details) are represented by stars for *n*-nonane and squares for *n*-propanol.

0.15 mN/m. The results are shown in Fig. 1 and appear to be in accordance with the expressions from Dean.[33] The applicability for these expressions is specified for the temperature ranges of 220–424 K for *n*-nonane and 147–371 K for *n*-propanol, with an uncertainty estimated to approximately ±0.1 mN/m (0.35).

For the situation where no experimental data for surface tensions of mixtures are available, several theoretical prediction methods can be used, based on pure component properties and the composition of the mixture.

In Fig. 2 are plotted the surface tensions of the *n*-propanol–*n*-nonane mixture at 293.15 K estimated in two different ways. Using the ideal solution theory, the mixture surface tension increases linearly with increasing *n*-nonane mole fraction while the method of Winterfield, Scriven, and Davis[38] (WSD) will show a nonlinear trend. The WSD equation for a nonaqueous solution of *n* components is

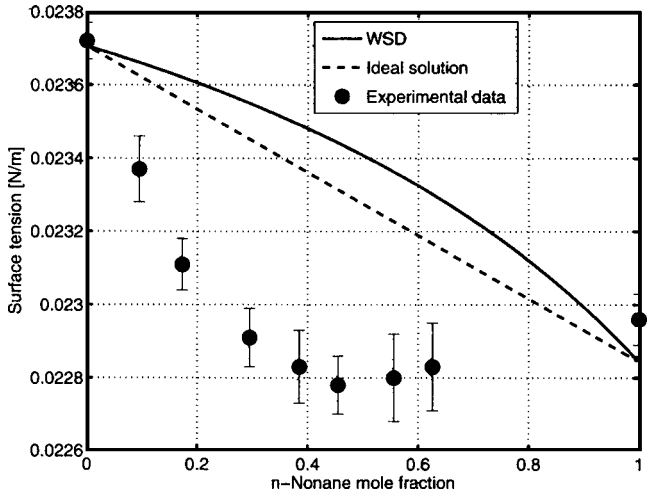

FIG. 2. Surface tension of *n*-nonane–*n*-propanol mixture at 293.15 K calculated using ideal solution theory (dashed line) and Winterfeld, Scriven, and Davis method (solid line). Our experimental surface tension for the mixture is represented by circles.

$$\sigma_{\mathrm{mix}} = \sum_{1=i}^{n} \sum_{j=1}^{n} \rho^2 \left(\frac{x_i}{\rho_{Li}}\right)\left(\frac{x_j}{\rho_{Lj}}\right)(\sigma_i \sigma_j)^{1/2}, \tag{21}$$

$$\frac{1}{\rho} = \sum_{i=1}^{n} \frac{x_i}{\rho_{Li}}, \tag{22}$$

where σ_{mix}=mixture surface tension, mN/m; $\rho_{Li,j}$=pure component liquid density, kmol/m^3; $\sigma_{i,j}$=pure component surface tension, mN/m; and $x_{i,j}$=component *i* or *j* mole fraction in the liquid mixture. This method can be used for almost all organic mixtures, with typical deviations of 3%–4% from the experimental points.

Surface tensions for mixtures of *n*-nonane and *n*-propanol at 293.15 K were measured in the present study using the same method as described above for pure components. The experimental results are indicated in Fig. 2 and show significant deviations from the above-mentioned theoretical predictions. The experimental curve displays an apparent minimum at about 0.45 *n*-nonane mole fraction, leading to the conclusion that *n*-nonane is surface active at low *n*-nonane mole fractions while *n*-propanol assumes a weak surface active role when the bulk mixture is rich in *n*-nonane. According to Papaioannou and Panayioutou[39] who conducted several studies on the thermophysical properties of hydrogen-bonded systems, in an alkanol-alkane mixture there are two factors which force the alkanol (*n*-propanol in our case) to avoid the surface: the lower surface tension of the alkane (here *n*-nonane) and the fact that the hydrogen bonding interaction is accomplished more efficiently in the bulk than the surface. In principle, alkanols (e.g., *n*-propanol) associate strongly in both pure state and in mixture while alkanes (e.g., *n*-nonane) play the role of inert "solvents" who are just reducing the degree of hydrogen bonding in the mixture. This probably explains why the interfacial region is rich in alkane rather than alkanol, especially in the alkanol rich compositions. On the other hand, upon adding more alkane in the mixture, the alkanol will tend to move on the interface where there are less alkane molecules able of breaking the structure of the hydrogen-bonded alkanol chains.

The WSD surface-tension prediction method gives a completely different result compared to experiments, and it cannot be applied for this particular mixture. Therefore a different model based on the generalized Langmuir equation has been applied.[40] The model uses the bulk volume fractions and has an adjustable parameter β accounting for the lyophobicity (solvent repellence) of one the components. The general equation can be written as

$$(\sigma - \sigma_1)/(\sigma_2 - \sigma) = \beta \phi_2/\phi_1, \tag{23}$$

where σ is the surface tension of the solution, σ_1 and σ_2 are the pure component surface tensions (here we used the expressions from Dean), $\phi_2/\phi_1 = (x_2 v_2)/(x_1 v_1)$ is the ratio of the occupation, x_i is the mole fraction of component *i*, v_i is the molar volume, and $\beta = k_{\mathrm{ads}}/k_{\mathrm{des}}$ with k_{ads} and k_{des} being the rate constants related to adsorption and desorption velocities. The value for β has been obtained by fitting Eq. (20) to the experimental data points for 293.15 and 273.15 K. For both temperatures β was found to be 0.1379. Using Eq. (20),

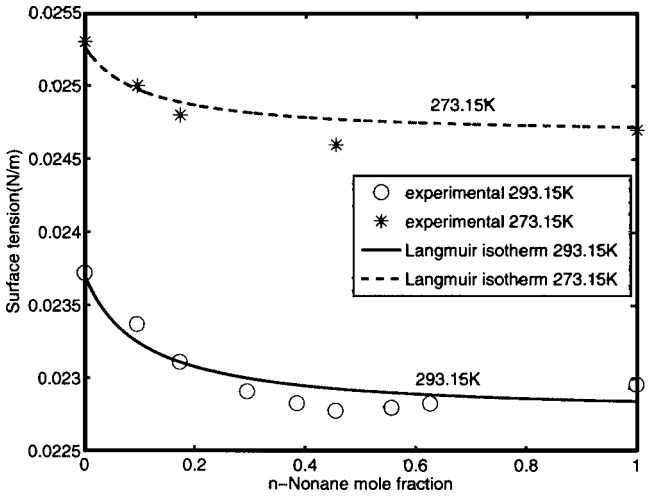

FIG. 3. Experimental surface tension of *n*-nonane–*n*-propanol mixture at 293.15 K (circles) and 273.15 K (stars) and the fitted extended Langmuir isotherms with $\beta=0.1379$ (solid line for 293.15 K and dashed line for 273.15 K).

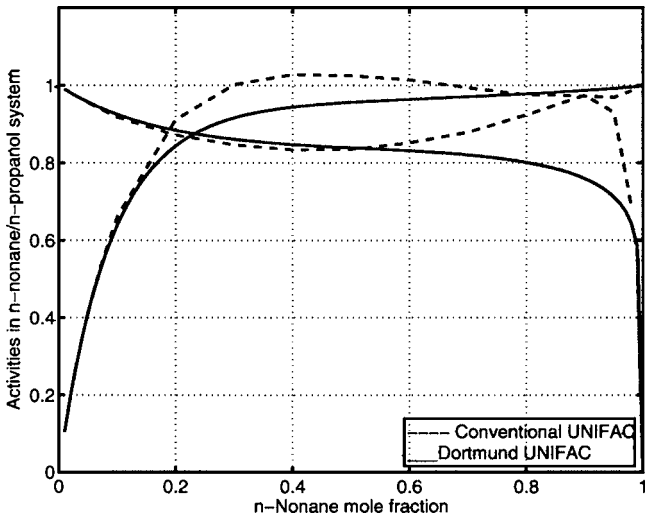

FIG. 4. UNIFAC Dortmund (solid lines) and original UNIFAC (dashed lines) activities of *n*-nonane and *n*-propanol as a function of *n*-nonane mole fraction at temperature $T=230$ K.

the surface tension of the mixture at 230 K can be determined. Figure 3 shows the experimental points for both temperatures together with the Langmuir isotherms. Although the Langmuir isotherms are not able to reproduce the observed minimum of surface tension, the overall fit to the experimental points can be considered reasonably good.

D. Activity coefficients

The activity (A_i) of a component i in liquid phase at certain temperature (T), pressure (p), and composition (x) is defined as

$$A_i(T,p,x)=\frac{f(T,p,x)}{f_0(T,p_0,x_0)}, \tag{24}$$

where $f(T,p,x)$ is the fugacity at the same conditions as A_i and $f(T,p,x)$ is the fugacity in standard state, that is the state at the same temperature as the mixture but at some arbitrary but specified conditions of composition and pressure (x_0 and p_0, respectively). In general, it is useful to chose the pure component as the standard state and to calculate the activity coefficient using the simplified expression,

$$A_i=\frac{P_{\mathrm{sat},i}(x_i,T)}{P^0_{\mathrm{sat},i}(T)}, \tag{25}$$

where $P_{\mathrm{sat},i}(x_i,T)$ is the saturation vapor pressure of component i over a flat surface of mixture and $P^0_{\mathrm{sat},i}(T)$ is the saturation vapor pressure of i over a flat surface of pure component and x_i. The activity coefficient γ_i is defined as the ratio of the activity of component i to some convenient measure of concentration (in the present paper mole fraction),

$$\gamma_i=\frac{A_i}{x_i}=\frac{P_{\mathrm{sat},i}(x_i,T)}{P^0_{\mathrm{sat},i}(T)x_i}. \tag{26}$$

To avoid any confusion that might arise from the similarity of the words, we present here the definition of the activity in gas phase,

$$a_i=\frac{P_{i,g}}{P^0_{\mathrm{sat},i}(T)}, \tag{27}$$

where $P_{i,g}$ is the partial vapor pressure of component i. Henceforth, a_i will stand only for gas phase activity.

Literature presents various methods for calculating/predicting the activity coefficients. Some of them require few experimental data for fitting the parameters and calculating the activity coefficients over the whole range of composition, while others are purely predictive methods. The universal functional activity coefficient (UNIFAC) model has been found to be useful for predicting thermodynamic properties, including activity coefficients.[41] This method requires group interaction parameters which are mainly fitted to experimental vapor-liquid equilibrium data. However, poor results are obtained when predicting the activity coefficients at infinite dilution or when the different molecular components in the system are very different in size.

The Dortmund version[42] is considered superior to UNIFAC and to other modified UNIFAC versions, particularly because more reliable activity coefficients at infinite dilution were obtained. Without getting into details, we mention that Dortmund UNIFAC uses a modified combinatorial part for dealing with components of very different sizes; several more main groups were added and the van der Waals properties were changed, introducing at the same time temperature-dependent parameters for a better description of activity coefficients as a function of temperature.

For comparison reasons only, both conventional UNIFAC and the Dortmund version were considered for evaluation of the activity coefficients in the *n*-nonane–*n*-propanol mixture (Fig. 4). The original UNIFAC introduces a small hump in the activity in liquid phase versus composition plot, suggesting a miscibility gap in the mixture somewhere between 0.4 and 0.84 *n*-nonane mole fraction. Experiments do not indicate any phase separation in this system, not even at as low a temperature as 230 K.[9] This apparent miscibility gap would introduce big errors in the nucleation rate calculations. The Dortmund UNIFAC activity in liquid phase

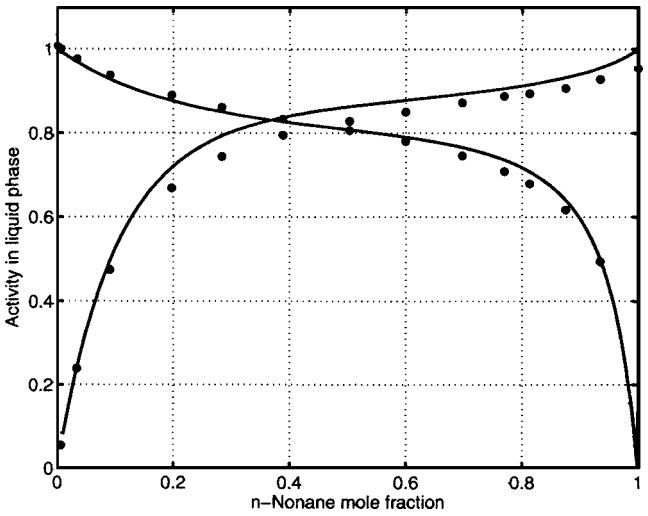

FIG. 5. Data of Goral *et al.* (Ref. 43) and UNIFAC Dortmund activities of *n*-nonane and *n*-propanol as a function of *n*-nonane mole fraction. Temperature is 333.15 K.

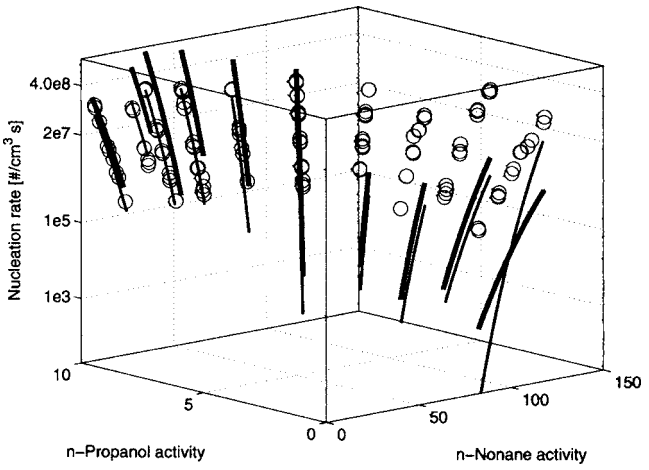

FIG. 6. Three-dimensional (3D) representation of the measured nucleation rates (circles) and theoretical rates CNT(Z2) (thin solid lines) and CNT(Z1) (thick solid lines) for eight different activity fractions (0, 0.0208, 0.0375, 0.0562, 0.0814, 0.118, 0.174, 0.256, 0.331, and 1). The activity fraction $f=1$ corresponds to pure propanol.

curve on the other hand does not exhibit any hump. The three data sets of activities in liquid phase in the propanol-nonane system presented by Goral *et al.*[43] at different *P-T-x-y* (pressure-temperature-mole fraction in liquid phase-mole fraction in gas phase) conditions enabled a comparison with the corresponding calculated curves by UNIFAC Dortmund. Figure 5 shows such a comparison for a temperature of 333.15 K. The good agreement gave us an additional reason to assume that the calculated activities at 230 K are in the proximity of the real values.

IV. RESULTS AND DISCUSSIONS

In their experimental work, Viisanen *et al.*[9] measured the nucleation rate as a function of vapor-phase activities a_1 and a_2 (henceforth referred to as activity) of the two components (see Appendix for the definition of vapor-phase activity). The ratio of the two activities a_2/a_1 remains constant during each experiment, only the total pressure and the individual activities are changed. The experimental nucleation rates were considered as a function of activity fraction defined as

$$f=\frac{a_2}{a_1+a_2}. \tag{28}$$

Also a normalized activity fraction of the vapor was considered, defined as

$$f_n=\frac{a_{2,n}}{a_{1,n}+a_{2,n}}, \tag{29}$$

where the $a_{i,n}$ represents the normalized vapor-phase activities,

$$a_{i,n}=\frac{a_i}{a_i^0}, \tag{30}$$

with a_i^0 the onset activities for the corresponding pure vapors. The nucleation temperature during the nucleation pulse was calculated as a function of chamber temperature and average pressure expansion ratio and found to be on average 230 K.

The above nucleation temperature together with the activities and activity fractions were used in our numerical calculations. A three-dimensional representation of experimental and theoretical nucleation rates is shown in Fig. 6. Each set of points represents the measured nucleation rate for a certain activity fraction; the thick solid lines show predictions of the classical nucleation theory with the accurate kinetics [CNT(Z1)], and the thin solid lines represent the classical nucleation theory with approximate kinetics CNT(Z2). One can see that both theoretical estimations are accurate enough for higher activity fractions (i.e., for low *n*-nonane gas phase activity) but present relatively large deviations as the activity fraction decreases. CNT(Z1) slightly overestimates the experiments on the propanol rich side but leads to a significant improvement on the nonane side, in particular, for pure nonane, by correcting the slope of nucleation rate versus activity curve.

In order to visualize the magnitude of the CNT deviations more clearly, two-dimensional plots of nucleation rates versus either *n*-nonane activity or *n*-propanol activity are presented in Fig. 7. Figure 7(a) presents the experimental and calculated [CNT(Z2)] nucleation rates as a function of *n*-nonane activity corresponding to $f=0$ (pure *n*-nonane), $f=0.0208$, and $f=0.0814$ activity fractions (only three activity fractions were selected for clarity). The numbers on the top of each curve represent an average factor required to bring the classical nucleation theory into approximate agreement with the experimental points. The correction factor needed for the CNT(Z2) nucleation rate prediction corresponding to the lowest five activity fractions is between 2×10^2 and 10^3.

Figure 7(b) on the other hand shows the nucleation rates [CNT(Z2)] for which no correction is needed (again, only three selected for clarity), corresponding to $f=0.118$, $f=0.256$, and $f=1$ (pure *n*-propanol) activity fractions. For this case also the slopes of the curves are essentially correct, while for the ones shown in Fig. 7(a) the slopes of the ex-

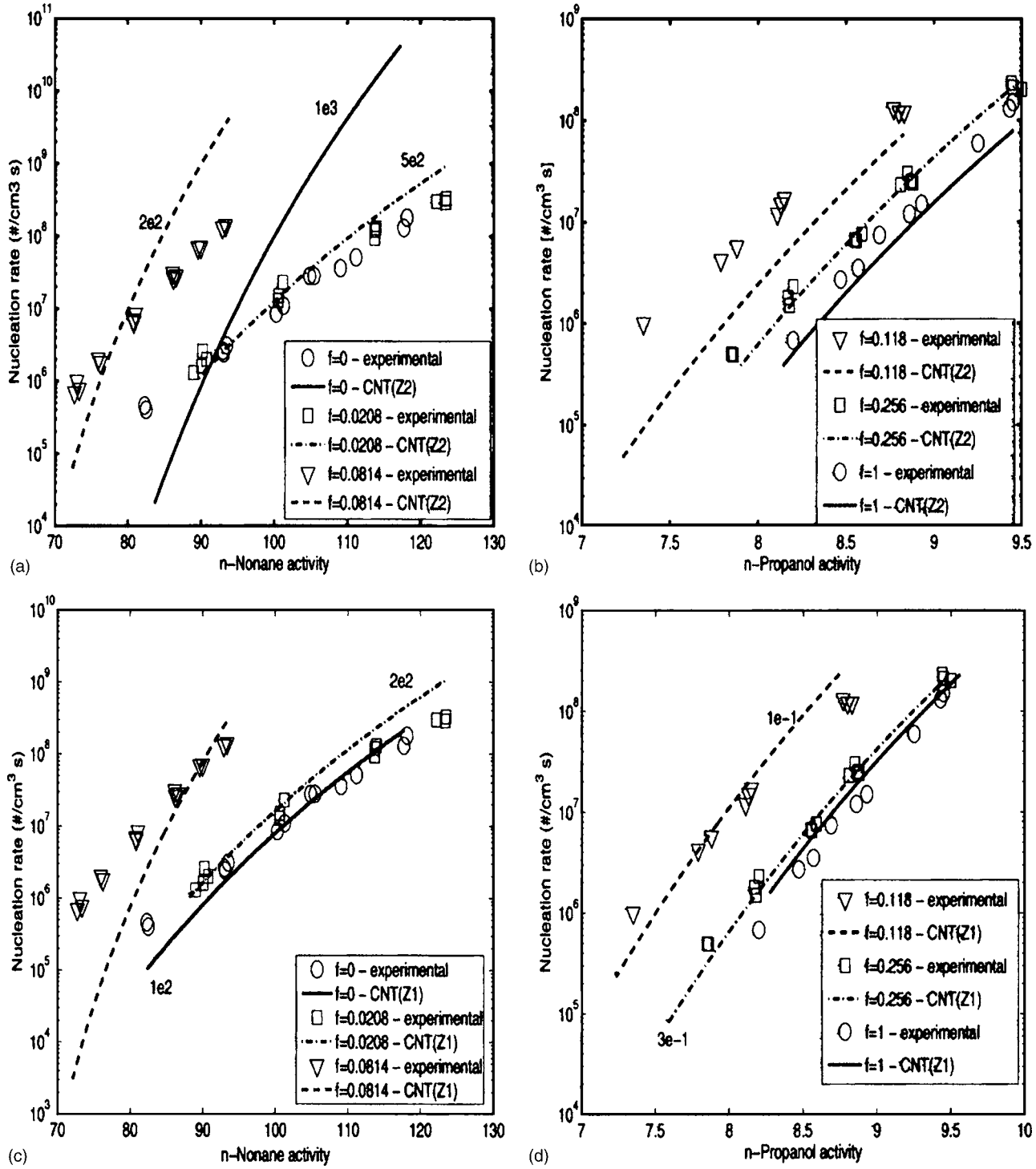

FIG. 7. Two-dimensional (2D) representation of the measured nucleation rates (circles, triangles, and squares) and theoretical rates (lines) as a function of *n*-nonane (a) and *n*-propanol (b) gas phase activities. Only six activity fractions were selected for clarity. The numbers indicated at the curves shown in (a) represent factors by which the CNT predictions were multiplied. Figures (a) and (b)—CNT(Z2); figures (c) and (d)—CNT(Z1).

perimental results decrease slower than the theoretical curves. Because the slopes are related to the number of molecules in the critical cluster, we expect that this quantity is accurately predicted by the theory for those clusters which correspond to curves with no correction factor. Similarly, the CNT(Z1) nucleation rate prediction are depicted in Figs. 7(c) and 7(d). CNT(Z1) brings an evident improvement, by lowering with about one factor of magnitude the difference between experiments and theory and by remedying the nucleation rate slope for pure nonane. Nevertheless, CNT(Z1) does not succeed in correcting the slope for the nucleation rate at $f=0.0814$.

The theoretical nucleation rates of pure *n*-nonane versus vapor-phase activity presented in Wagner and Strey[10] deviate from the experiments with a factor of 2000, while the correction factor applied to our CNT nucleation rate predictions is either 1000 or 100, depending on what kinetic prefactor has been used. The slopes of the theoretical curves in Wagner

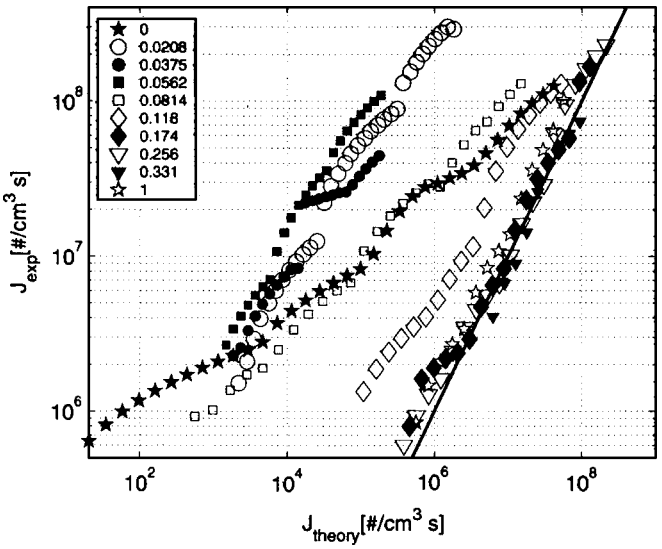

FIG. 8. Measured nucleation rates [CNT(Z2)] vs theoretical results at 230 K. The activity fractions related to each data set are given in the legend. The 1:1 line is plotted for comparison.

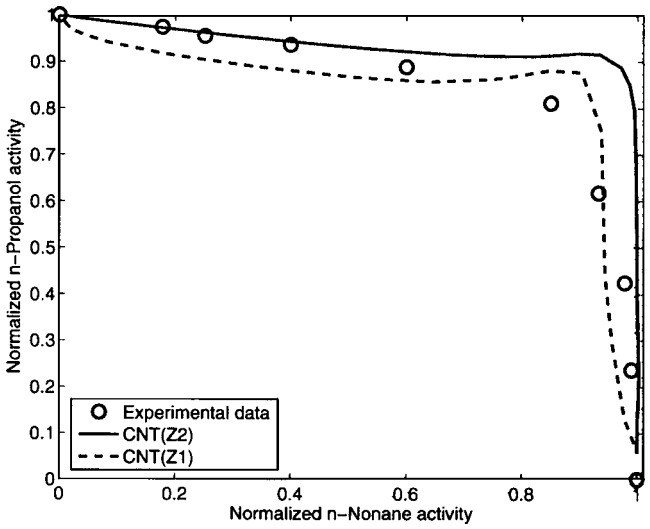

FIG. 10. Normalized vapor-phase activities (defined as the actual gas phase activity divided by the onset activities for the corresponding pure vapors) required for a constant nucleation rate of $10^7/\mathrm{cm}^3$ s.

and Strey[10] are found to be in good agreement with the experiments, a behavior which is consistent with our findings when using CNT(Z1) but not consistent for CNT(Z2).

A very straightforward and sensitive way of comparing the theory with the experimental data is to plot the experimental result against the theoretical predictions. Such a plot is presented in Fig. 8 [shown only for CNT(Z2)]. If the agreement between experiment and theory would have been perfect, all the data points would fall on the 1:1 solid line. The classical nucleation theory and the experiments agree at the highest four activity fractions, the data points laying comfortably close to 1:1 line. The discrepancy increases with the decreasing activity fraction of *n*-propanol.

We consider now the onset activities of *n*-nonane and *n*-propanol corresponding to a constant nucleation rate of $10^7/\mathrm{cm}^3$ s. Figure 9 presents the measured onset activities

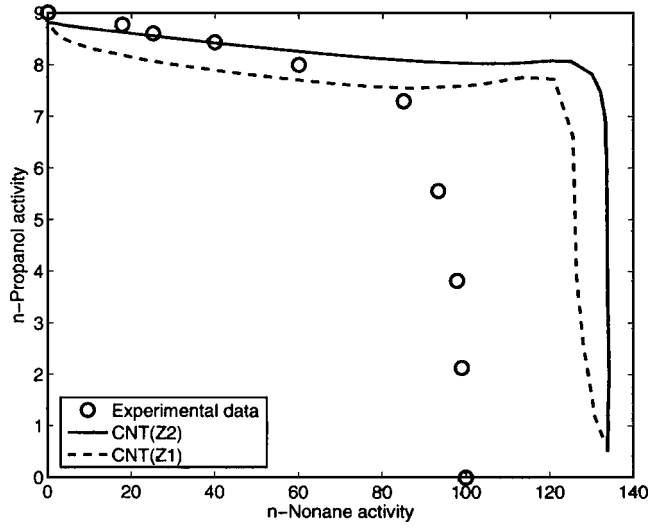

FIG. 9. The vapor-phase activities required to obtain a constant nucleation rate of $10^7/\mathrm{cm}^3$ s. CNT(Z2) (solid line) and CNT(Z1) (dashed line) calculations are compared with the experimental values of Viisanen *et al.* (Ref. 9) (circles).

together with the CNT(Z1) and CNT(Z2) predictions. There is a quantitative agreement between experiment and the theoretical CNT(Z2) curves on the side of low *n*-nonane activity (roughly up to 60). CNT(Z1) succeeds less well for low *n*-nonane concentrations by underestimating the experiments but overall appears to be closer to the experimental values than CNT(Z2). Above the value of 60 for *n*-nonane activity, the departure from the experimental data is increasing for both theoretical curves, exhibiting large discrepancies on the *n*-nonane rich side. First of all, experimental as well as theoretical curves of constant nucleation rate bend away from the origin. The theoretical curves, however, bend even stronger, having almost a 90° angle, which suggests that these two vapors might nucleate separately. Figure 10, where the onset activities for pure components are normalized to 1, better illustrates the different shapes of the theoretical and experimental curves. Moreover, one can also clearly see that the modeled onset activity curve displays a local maximum (a small "hump"), a behavior that has been seen before in some theoretical water-alcohol activity curves.[44,45] The behavior is strange and, according to Laaksonen *et al.*,[25] it is related to the assumption that the equimolar surface coincides with the surface of tension, which is unjustified for a surface active system.

As mentioned in Sec. III C, the uncertainties in Dean's expressions for *n*-nonane and *n*-propanol surface tensions are evaluated at 0.1 mN/m (representing 0.35% variation). Varying the pure component surface tensions with the above percentage will introduce a variation of the mixture surface tension of only 0.07%. On the other hand, the Langmuir isotherms overestimate the experiments with about 0.8% for both temperatures (see Fig. 3) in the region where the experimental data display a minimum. Because the experimental curves have a similar trend at both temperatures, it is reasonable to assume that the general appearance of the mixture surface tension curves at 230 K will be maintained and the uncertainty inserted by the Langmuir equation will not exceed 0.8%. A sensitivity analysis has been carried out by

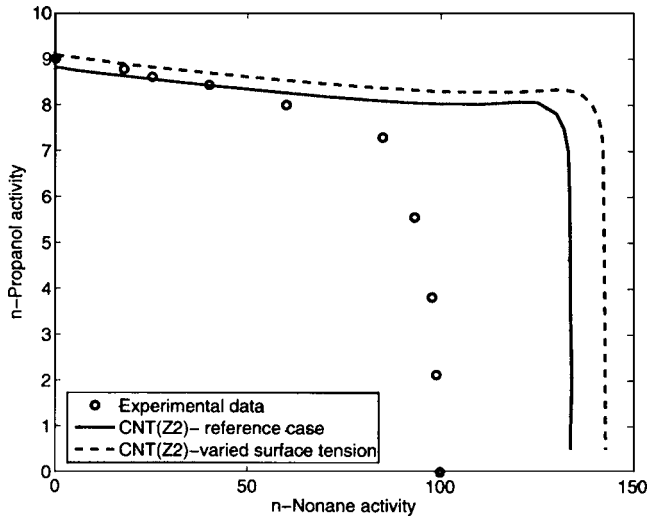

FIG. 11. The onset vapor-phase activities in the reference case (solid line) and with a 1% increased surface tension (dashed line). The experimental data (circles) are also presented.

increasing the surface tension of the mixture by 1%, and the onset activities corresponding to a constant nucleation rate of $10^7/\mathrm{cm}^3\,\mathrm{s}$ have been calculated. The new estimated values for the onset activities (Fig. 11) are about 3.3% higher on the horizontal part of the curve, increasing to 6.7% on the vertical side. This effect emphasizes the sensitivity of the nucleation process to minor perturbations of surface tension.

The number of molecules (*n*-nonane and *n*-propanol) in the critical cluster is presented in Fig. 12(a), where the experimental values of Viisanen *et al.*[9] and both the calculated CNT(Z2) core number of particles $n_{i,l}$ and the total number of particles $n_i=n_{i,l}+n_{i,s}$ are shown as separate lines. For evaluating the cluster composition, Viisanen *et al.*[9] used the slopes of the nucleation rate surface,

$$n_i \simeq \left.\frac{\partial \ln I}{\partial \ln a_i}\right|_{a_{j\neq i}}, \tag{31}$$

where I is the nucleation rate and a_i refers to the activity in gas phase of component i. The way the experiments have been conducted do not permit the direct use of the above expression. However, with the help of the onset activity curve which gives $(\partial a_2/\partial a_1)|_{I=\mathrm{const}}$ and the nucleation curve as a function of the average activity $a=\sqrt{(a_1^2+a_2^2)}$ which provides the slope $(\partial \ln I/\partial \ln a)|_{f=\mathrm{const}}$ [f defined in Eq. (28)], Eq. (31) can be written as

$$\left.\frac{\partial \ln I}{\partial \ln a_1}\right|_{a_2} = a_1\frac{\partial \ln I}{\partial a_1} = -a_1^0\left[\frac{\partial a_2}{\partial a_1}\right]_I\left[\frac{\partial \ln I}{\partial a}\right]_f \times\left[1+\left(\frac{a_2^0}{a_1^0}\right)^2\right]^{1/2}\Bigg/\left.\left[\frac{a_2^0}{a_1^0}-\frac{\partial a_2}{\partial a_1}\right]\right|_I. \tag{32}$$

Similarly,

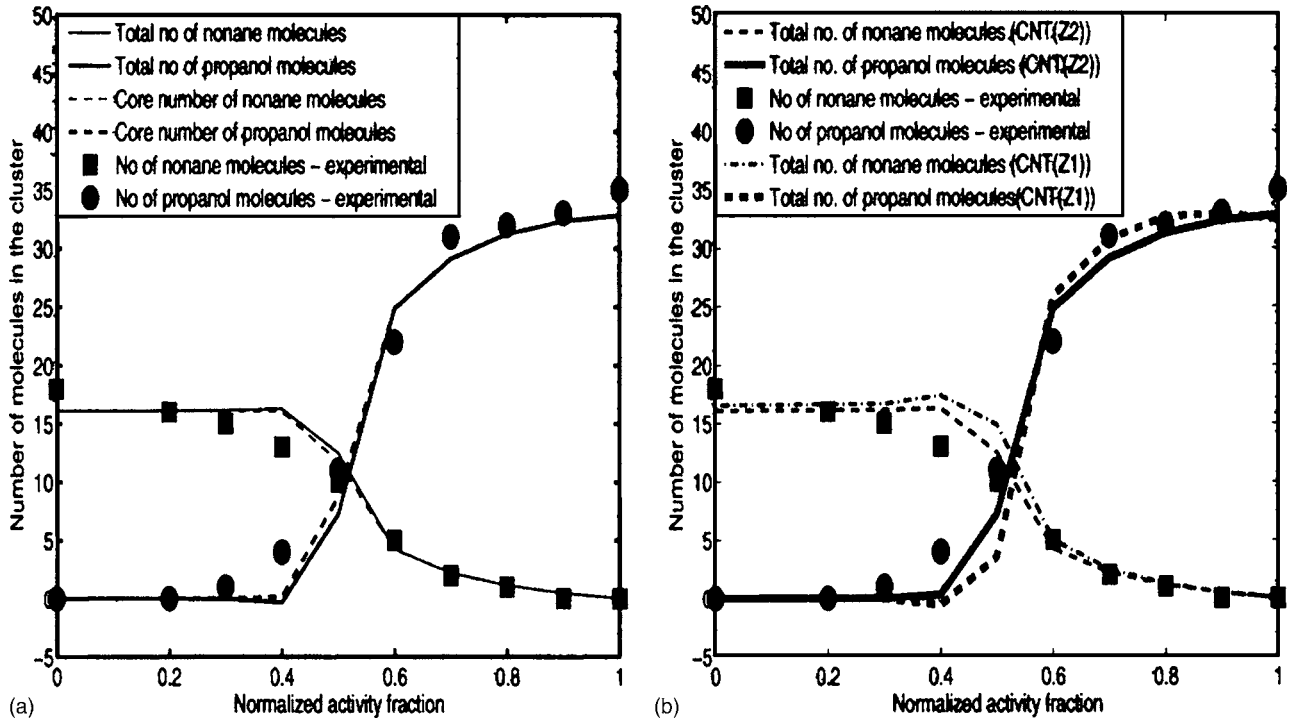

FIG. 12. Number of particles in the critical cluster as a function of normalized activity fraction. (a) The total number of particles and the core number of particles are shown along with experimental results of Viisanen *et al.* (Ref. 9) (b) Total number of *n*-nonane and *n*-propanol in the critical cluster from both CNT(Z2) and CNT(Z1).

$$\left.\frac{\partial \ln I}{\partial \ln a_2}\right|_{a_1} = a_2 \frac{\partial \ln I}{\partial a_2} = a_2^0 \left[\frac{\partial \ln I}{\partial a}\right]_f \times \left[1+\left(\frac{a_2^0}{a_1^0}\right)^2\right]^{1/2} \Bigg/ \left.\left[\frac{a_2^0}{a_1^0} - \frac{\partial a_2}{\partial a_1}\right]\right|_I . \quad (33)$$

For a more detailed argumentation, we direct the reader to the work of Strey and Viisanen.[11]

The surface excess number of molecules $n_{i,s}$ are calculated using the Eqs. (7) and (8). The surface excess numbers of molecules are sensitive indicators of the failure of CNT; they should be a minor correction to $n_{i,l}$ rather than a dominating contribution for the theory to be valid. For example, in the water-ethanol system, the $n_{i,s}$ values are large and can render the total number of water molecules negative.[4] Figure 12(a) presents the measured cluster composition (full points and squares) in comparison with the theoretical—CNT(Z2)—values for total and core numbers of molecules. It can be seen from Fig. 12(a) that in our case the number of molecules is quite accurately approximated by $n_{i,l}$, i.e., the surface excess is small, which suggests that CNT might perform quite well for the *n*-nonane–*n*-propanol system. Around $a_{1,n}=0.4$, n_2 is negative but small, in practice zero. The largest differences between n_i and $n_{i,l}$ are about one molecule. The deviations from experimental values between normalized activity fractions of 0.4 and 0.7 are considerable. This reflects the fact that the composition change in small clusters as a function of mole fraction is more gradual than predicted by CNT(Z2). Even so, the total number of molecules (n_1+n_2) (not shown) is rather close to experimental values also at medium compositions.

The effect of the expression for the kinetic prefactor on the theoretically obtained cluster composition is illustrated in Fig. 12(b) where the total number of molecules calculated with CNT(Z2) and CNT(Z1) is shown. Both theoretical predictions have similar trends, aside from the fact that CNT(Z1) has the tendency of departing more from the experimental compositions. We also calculated the numbers of molecules in a similar fashion as Viisanen *et al.*, i.e., using Eqs. (31)–(33). The results agree with the ones calculated from Eqs. (5)–(8) (apart from small errors resulting from numerical derivatives). This is not surprising because classical nucleation theory is consistent with the nucleation theorem.

V. CONCLUSIONS

Experimental data and CNT calculations on the binary nucleation of the *n*-nonane–*n*-propanol system have been compared. The importance of the kinetic prefactor has been also considered. Various thermodynamical data have been considered, emphasizing the fact that high accuracy is required for the correct prediction of nucleation rates. This is especially true for surface tension and activity coefficients since the theoretical nucleation rates are extremely sensitive to their variation.

Classical nucleation theory predicts fairly well the nucleation rates in *n*-nonane–*n*-propanol system for low nonane and high *n*-propanol activities. Increasing the *n*-nonane activity in gas phase leads to a departure of the theoretical nucleation rates from the experimental values by about two orders of magnitude in case of classical nucleation theory with accurate kinetic prefactor and with more than three orders of magnitude in case of CNT with approximate prefactor. Overall, CNT(Z1) brings a certain improvement by correcting the slope of the nucleation rate surface for pure *n*-nonane and by reducing the difference between theory and experiments.

But the strange behavior of CNT at intermediate vapor compositions indicates problems with the theory. The systematic departure of the theoretical onset activities from the experimental data for smaller concentrations of *n*-propanol could be caused by an incorrect parametrization of some thermophysical property. Also, the fact that the *n*-nonane–*n*-propanol system is surface active might be the reason of the "hump" in the theoretical activity curves. The error may also be attributed to the use of bulk thermophysical values when small clusters are considered. For a constant nucleation rate of 10^7 cm^{-3} s^{-1} the pure *n*-propanol cluster contains about 32 molecules, whereas a pure *n*-nonane cluster has only about 16 molecules. The CNT values are likely to depart most from the experimental values for small clusters. This effect is compounded by the different sizes of the molecules. Both *n*-propanol and *n*-nonane are chainlike molecules, but the length of an *n*-propanol molecule is about 6 Å as opposed to 10 Å for an *n*-nonane molecule.[46] We then expect for the density and surface tension of small clusters to be in greater discrepancy with the bulk values for *n*-nonane than for *n*-propanol because longer molecules are not likely to settle into a bulklike configuration in the cluster, owing to, for example, excluded volume effects. Although nonane and propanol are fully miscible at all proportions, the nucleation experiments indicate only reluctant conucleation. According to onset activity curves (Fig. 9) and the composition of the critical cluster (Fig. 11), this behavior is now well represented by the classical nucleation theory as well. Anyhow, a more detailed analysis of the differences between the experiments and the predictions by CNT would require more accurate data on the thermophysical properties of *n*-nonane–*n*-propanol solution.

ACKNOWLEDGMENTS

Academy of Finland is gratefully acknowledged for the financial support. Part of this work was supported by the Austrian Science Foundation (FWF, Project No. P16958-N02) and by the Hochschuljubiläumsstiftung of the City of Vienna.

[1] M. Volmer and A. Weber, Z. Phys. Chem. **119**, 277 (1926).
[2] J. Frenkel, *Kinetic Theory of Liquids* (Oxford University Press, London, 1946).
[3] J. Zeldovich, Acta Physicochim. URSS **18**, 1 (1943).
[4] K. Neumann and W. Döring, Z. Phys. Chem. Abt. A **186**, 203 (1940).
[5] D. Stauffer, J. Aerosol Sci. **7**, 319 (1976).
[6] H. Trinkaus, Phys. Rev. B **27**, 7372 (1983).

[7] R. Strey, Y. Viisanen, and P. E. Wagner, J. Chem. Phys. **103**, 4333 (1995).
[8] Y. Viisanen and R. Strey, J. Chem. Phys. **105**, 8293 (1996).
[9] Y. Viisanen, P. E. Wagner, and R. Strey, J. Chem. Phys. **108**, 4257 (1998).
[10] P. Wagner and R. Strey, J. Phys. Chem. B **105**, 11656 (2001).
[11] R. Strey and Y. Viisanen, J. Chem. Phys. **99**, 4693 (1993).
[12] C. Hung, M. J. Krasnopoler, and J. L. Katz, J. Chem. Phys. **90**, 1856 (1989).
[13] A.-P. Hyvärinen, H. Lihavainen, Y. Viisanen, and M. Kulmala, J. Chem. Phys. **120**, 11621 (2004).
[14] A. I. Gaman, M. Kulmala, H. Vehkamäki, I. Napari, M. Mircea, and M. C. Facchini, J. Chem. Phys. **120**, 282 (2004).
[15] R. Kamens, M. Jang, C. Chien, and K. Leach, Environ. Sci. Technol. **33**, 1430 (1999).
[16] I. Napari, M. Kulmala, and H. Vehkamäki, J. Chem. Phys. **117**, 8418 (2002).
[17] D. Wright and M. S. El-Shall, J. Chem. Phys. **98**, 3369 (1993).
[18] D. Wright, R. Caldwell, C. Moxley, and M. S. El-Shall, J. Chem. Phys. **98**, 3356 (1993).
[19] M. Rusyniak and M. S. El-Shall, J. Phys. Chem. B **105**, 11873 (2001).
[20] G. W. Adams, J. L. Schmitt, and R. A. Zalabsky, J. Chem. Phys. **81**, 5074 (1984).
[21] H. Reiss, J. L. Katz, and E. R. Cohen, J. Chem. Phys. **48**, 5553 (1968).
[22] H. Reiss and J. L. Katz, ARPA Technical Report (unpublished).
[23] M. Kulmala, A. Lauri, H. Vehkamäki, A. Laaksonen, D. Petersen, and P. E. Wagner, J. Phys. Chem. B **105**, 11800 (2001).
[24] P. E. Wagner, D. Kaller, A. Vrtala, A. Lauri, M. Kulmala, and A. Laaksonen, Atmos. Chem. Phys. **3**, 89 (2003).
[25] A. Laaksonen, R. McGraw, and H. Vehkamäki, J. Chem. Phys. **111**, 2019 (1999).
[26] M. Noppel, H. Vehkamäki, and M. Kulmala, J. Chem. Phys. **116**, 218 (2002).
[27] K. Binder and D. Stauffer, Adv. Phys. **25**, 343 (1976).
[28] H. Reiss, J. Chem. Phys. **18**, 840 (1950).
[29] M. Kulmala and Y. Viisanen, J. Aerosol Sci. **22**, S97 (1991).
[30] *Chemical Properties Handbook*, edited by C. Yaws (McGraw-Hill, New York, 1999).
[31] M. King and H. Najjar, Chem. Eng. Sci. **29**, 1003 (1974).
[32] T. Schmeling and R. Strey, Ber. Bunsenges. Phys. Chem. **87**, 871 (1983).
[33] *Lange's Handbook of Chemistry*, 15th ed., edited by J. Dean (McGraw-Hill, New York, 1999).
[34] P. E. Wagner and R. Strey, J. Chem. Phys. **80**, 5266 (1984).
[35] R. Strey and T. Schmeling, Ber. Bunsenges. Phys. Chem. **87**, 324 (1983).
[36] R. Dettre and R. J. Johnson, J. Colloid Interface Sci. **21**, 367 (1966).
[37] A. Adamson, *Physical Chemistry of Surfaces*, 5th ed. (Wiley, New York, 1990).
[38] P. H. Winterfeld, L. E. Scriven, and H. T. Davis, AIChE J. **24**, 1010 (1978).
[39] D. Papaioannou and C. Panayiotou, J. Chem. Eng. Data **39**, 457 (1994).
[40] A. Pineiro, P. Brocos, A. Amigo, J. Gracia-Fadrique, and M. G. Lemus, Langmuir **17**, 4261 (2001).
[41] A. Fredenslund, R. Jones, and J. Prausnitz, AIChE J. **21**, 1086 (1975).
[42] J. Gmehling, D. Tiegs, and U. Knipp, Fluid Phase Equilib. **54**, 147 (1990).
[43] M. Goral, P. Oracz, A. Skrzecz, A. Bok, and A. Maczynski, J. Phys. Chem. Ref. Data **31**, 701 (2002).
[44] Y. Viisanen, R. Strey, A. Laaksonen, and M. Kulmala, J. Chem. Phys. **100**, 6062 (1994).
[45] R. Strey, P. E. Wagner, and Y. Viisanen, Proceedings of the 13th International Conference on Nucleation and Atmospheric Aerosols, 1992, edited by N. Fukuta and P. E. Wagner (A. Deepak, Hampton, VA, 1992), pp. 111–120.
[46] *CRC Handbook of Chemistry and Physics*, 83rd ed., edited by D. R. Lide (CRC, Boca Raton, FL, 2002).